EBSD characterization of graphene nano sheet reinforced Sn–Ag solder alloy composites

Shanthi Bhavan, J., Pazhani, A., Robi, P. S., Ambi, A., Tg, U. & Kc, V.

Published PDF deposited in Coventry University's Repository

Original citation:
Shanthi Bhavan, J, Pazhani, A, Robi, PS, Ambi, A, Tg, U & Kc, V 2024, 'EBSD characterization of graphene nano sheet reinforced Sn–Ag solder alloy composites', Journal of Materials Research and Technology, vol. 30, pp. 2768-2780.
https://dx.doi.org/10.1016/j.jmrt.2024.04.043

DOI 10.1016/j.jmrt.2024.04.043
ISSN 2238-7854
ESSN 2214-0697

Publisher: Elsevier

This is an open access article under the CC BY license
(http://creativecommons.org/licenses/by/4.0/)

Journal of Materials Research and Technology 30 (2024) 2768–2780

Contents lists available at ScienceDirect

Journal of Materials Research and Technology

journal homepage: www.elsevier.com/locate/jmrt

EBSD characterization of graphene nano sheet reinforced Sn–Ag solder alloy composites

Jayesh Shanthi Bhavan [a,*], Ashwath Pazhani [a], P.S. Robi [d], Abhishek Ambi [a], Unnikrishnan Tg [c], Vishnu Kc [b]

[a] School of Mechanical Engineering, Coventry University, Coventry, CV1 5FB, UK
[b] Centre for Manufacturing and Materials, Coventry University, CV1 5FB, UK
[c] Department of Engineering, Leicester College, Leicester, UK
[d] Department of Mechanical Engineering, Indian Institute of Technology Guwahati, 781039, India

ARTICLE INFO

Handling editor: P Rios

Keywords:
Graphene nano Sheets
Sn–Ag Solder alloys
Microstructural characterization
Electron Backscatter diffraction
Lead-free

ABSTRACT

This research explores the effects of incorporating Graphene Nano Sheets (GNS) on the microstructural characteristics and mechanical behavior of Sn–Ag solder alloys. The research was driven by the need for environmentally friendly, lead-free solder alloys with enhanced mechanical and thermal properties. The methodology involved incorporating graphene into the Sn–Ag alloy through stir casting, followed by a series of surface preparation techniques. The composite samples were then examined using EBSD to analyze crystallographic orientations and SEM/EDS for surface morphology and elemental composition. XRD provided insights into phase transformations and structural changes. Key findings reveal that the addition of GNS significantly refines the grain structure of the Sn–Ag alloy, leading to a bimodal grain size distribution. This refinement is attributed to the role of GNS as a nucleation site during solidification. Moreover, the study demonstrates a pronounced alteration in the texture of the material, with an increase in low-angle grain boundaries post-GNS addition. This texture change is indicative of enhanced mechanical properties. The results also show a shift in the orientation distribution function (ODF), suggesting a stronger crystallographic orientation due to GNS. These findings suggest that GNS incorporation could lead to improved mechanical and thermal properties in Sn–Ag solder, making them suitable for high-performance electronic applications. The study concludes that GNS not only serves as an effective reinforcement in Sn–Ag solder alloys but also significantly alters their microstructural and textural characteristics, contributing to the alloy's potential application in environmentally conscious electronic manufacturing.

1. Introduction

Soldering is a widely recognized metallurgical bonding technique employing a filler metal, known as solder, characterized by a melting point below 425 °C [1]. Solder serves as a bonding material, ensuring electrical, thermal, and mechanical continuity within electronic package assemblies [1]. Sn–Pb (67%–33% by wt.) was widely used and popular solder alloy [2]. Lead cannot be used in solder alloy making process anymore due to its inherent toxicity [3,4]. The ban on usage of Pb has been imposed following the legislation (as charted in the WEEE proposal [5]). Researchers around the globe started focusing their attention on development of new lead free solder alloys which can replace the traditional Sn–Pb alloy. In the binary system, the Sn–In solder with a eutectic temperature of 120 °C and composition of Sn–51In offers good wettability and a low melting point but suffers from poor plasticity and high cost [6]. The Sn–Bi type, with a eutectic temperature of 138 °C and Sn–57Bi composition, is characterized by high mobility but has issues with processability and low ductility [7,8].Sn–Zn solder, with a eutectic temperature of 198 °C and a composition of Sn–9Zn, is recognized for its high intensity and abundance, but it oxidizes easily and has poor wettability [9]. The Sn–Ag type, having a eutectic temperature of 221 °C and Sn-3.5Ag composition, is noted for its high strength and resistance to creep, but it has a high melting point and cost [10]. Sn–Cu solder, with a eutectic temperature of 227 °C and a Sn-0.7Cu composition, is also known for its high strength and creep resistance, and it is resourceful, but it suffers from a high melting point [11]. In the ternary

* Corresponding author.
E-mail address: ae0281@coventry.ac.uk (J. Shanthi Bhavan).

https://doi.org/10.1016/j.jmrt.2024.04.043
Received 18 February 2024; Received in revised form 28 March 2024; Accepted 6 April 2024
Available online 8 April 2024
2238-7854/© 2024 The Authors. Published by Elsevier B.V. This is an open access article under the CC BY license (http://creativecommons.org/licenses/by/4.0/).

system, the Sn–Ag–Cu solder, with a eutectic temperature of 217 °C and composition of Sn-3.5Ag-0.9Cu, is distinguished for its high strength and creep resistance but comes at a higher cost [12]. Lastly, the addition of granules like Ag, Al, Ga, Sb, carbon nanotubes, boron nitride nanotubes, and graphene nanosheets (GNSs) improves the melting point and mechanical properties of lead-free solders, as discussed in Ref. [13].

In one study, Composite SAC alloys were created using Sn99Ag0.3Cu0.7 alloy with 0.5 wt% TiO2 and SiC nano-particles. Solder joints were formed between two 150 μm thick Cu plates using SMT technology. This revealed an uneven distribution within the solder mass that varied with the particles' size and shape. DFT calculations confirmed that the non-soluble TiO2 and SiC could chemically bond with Sn during soldering, likely enhancing the SAC alloys' physical properties [14]. The enhancement of the Sn-3.0Ag-0.5Cu solder alloy's hardness, due to the addition of 1.0 wt% TiO2 nanoparticles, was assessed through nanoindentation tests. The inclusion of TiO2 nanoparticles led to a reduction in the size of the Cu6Sn5 and Ag3Sn intermetallic compound phases. With the incorporation of 1.0 wt% TiO2 nanoparticles, there was up to a 26.2% increase in hardness compared to the base SAC305 alloy [15].SiC nano-fibers and nano-particles, at a concentration of 0.5 wt%, were blended into the SAC0307 alloy. After storing the solder joints for 4000 h at 85 °C and 85% relative humidity, it was found that the SiC nano-phases reduced the corrosion resistance of the composite solder alloys and contributed to increased growth of Sn whiskers [16]. The impact of adding SiC nano-phases (particles and fibers) to SAC0307 solder paste on the thermal and microstructural characteristics of the solder joints was studied. At 0.5 wt%, SiC nano-particles improved the thermal properties of the joints. Microstructural examination showed that the refinement of the solder joints' structure varies between nano-particles and nano-fibers [17]. The effects of reinforcing Sn99Ag0.3Cu0.7 (SACX0307) solder alloy with ZnO nanoparticles were studied. ZnO nanoparticles reduced the alloy's wettability, leading to more voids. However, the shear strength and thermoelectric properties of the composite solder alloy remained unchanged [18]. Another study study focuses on detailed morphological analysis of TiO2 nanoparticles embedded in SAC305 through selective electrochemical etching. TiO2 nanoparticles at the solder interface inhibit the expansion of the Cu6Sn5 intermetallic compound (IMC) layer [19].

Graphene, a two-dimensional material made of carbon, is renowned for its exceptional electrical and thermal conducting properties and vast surface area. Over the past ten years, it has become one of the most extensively studied materials, finding applications across diverse domains [20,21].

Recent research has increasingly shown that incorporating graphene into metal-based composites significantly improves their electrical conductivity and mechanical strength [22,23]. Graphene has been utilized in the modification of existing Sn-based lead-free solder alloys. There are two variants of this graphene-enhanced lead-free solder: one is the standard version with unmodified graphene, and the other is a type that includes metal particle-treated solder. Initially, graphene was incorporated into the solder matrix to act as a reinforcement phase [24,25]. However, there is little information regarding the microstructure and mechanical properties of Sn–Ag alloy solders reinforced with Graphene Nano Sheets (GNS). Hence this work aims to thoroughly investigate the influence of Graphene Nano Sheets on the microstructure and mechanical properties of Sn–Ag solder alloys.

The primary objectives include analyzing the effects of GNS addition on grain size distribution, crystallographic texture, and phase composition by employing a combination of Electron Backscatter Diffraction (EBSD), Scanning Electron Microscopy (SEM), X-ray diffraction (XRD) and Energy Dispersive Spectroscopy (EDS). The seeks to understand how GNS incorporation alters solder alloy characteristics, particularly focusing on the development of crystallographic texture and its implications for mechanical properties. The research also aims to explore the potential mechanisms by which GNS affects the nucleation and growth of grains during the processing of Sn–Ag solder alloys, providing insights into the enhanced mechanical and thermal properties of these modified alloys.

2. Materials and methods

2.1. Sample preparation

Graphene is incorporated into the Sn–Ag alloy using the stir casting technique, which is a straightforward method for producing particulate-reinforced metal matrix composites (MMCs) in a liquid state. Sn–Ag alloy (96.5–3.5, % by wt.) is heated in a furnace till the temperature reaches 250 °C. The GNS is incrementally introduced into the molten matrix metal. GNS used for the study are a gray black powder with a specific surface area(m^2/g) of 50–200, greater than 80% single layer rate, a thickness of 1–3 layers (0.686–1.054 nm), and a diameter to thickness ratio of 9500. This mixture is mechanically stirred, using a graphite impeller, simultaneously to ensure uniform distribution. Effective stirring is crucial to achieve a homogeneous dispersion of the graphene particles within the molten matrix [26]. Following the stirring process, the composite mixture of reinforcement and molten matrix is cast in to a mold and allowed to cool to room temperature. Samples of 10 x 10 × 1 mm (5 samples) were made for further analysis. Fig. 1 shows the entire methodology adopted for this study.

The sample preparation method involves several steps using different abrasive materials and techniques. Initially, the surface of the sample is grinded with CarbiMet Silicon Carbide (SiC) paper at 600 and1200 grit until the surface becomes planar. The base rotation speed during this step is set at 150 rpm with a relative rotation in a consistent direction. Following this, the sample is further processed using TexMet-C with 3 μm Metadi Ultra Diamond paste and MetaDi Fluid but with a change in the relative rotation direction. Following the grinding process, the samples were subjected to a cleaning procedure using an Ultrasonic Cleaner. This involved a 5-min cleaning session with a solution consisting of 1% liquid soap. Post-cleaning, the samples underwent an inspection using an optical microscope at 50× magnification. The third step involves the use of ChemoMet/MasterTex with MasterPrep 0.05 μm Alumina under for the vibratory polishing for 60 min. The samples were secured in a specimen holder with a mass of 400 g, and no extra weights were added during this process. This comprehensive preparation method ensures a high-quality surface finish, suitable for detailed analysis and characterization.

2.2. XRD

The X-ray diffraction (XRD) analysis of Sn–Ag-GNS solder composite was conducted using a Powder Diffraction Standard method. XRD analysis was carried out on the top surface using a D8 Advance DaVinci system (Bruker, Coventry, UK) and a LYNXEYE detector. The wavelength of X-rays used was 1.5406 Å for Alpha1 and 1.54439 Å for Alpha2, with an average wavelength of 1.5418 Å. The scan was performed in a continuous PSD fast mode, with a time per step of 0.12 s and a total time per step of 23.04 s. The intensity vs 2θ data was obtained and recorded.

2.3. SEM and EDS methods

Scanning Electron Microscopy (SEM) and Energy Dispersive Spectroscopy (EDS) (Carl Zeiss Gemini) were utilized to investigate the surface morphology and elemental composition of Sn–Ag-GNS solder composite. SEM provided high-resolution imaging of the Sn phase and Ag_3Sn intermetallic compounds, and the influence of GNS on the microstructural evolution within the alloy. EDS complemented this by quantitatively analyzing the distribution of Sn and Ag and C elements. This combination of techniques was critical in understanding the composition and the formation of Ag_3Sn phases, which are crucial for

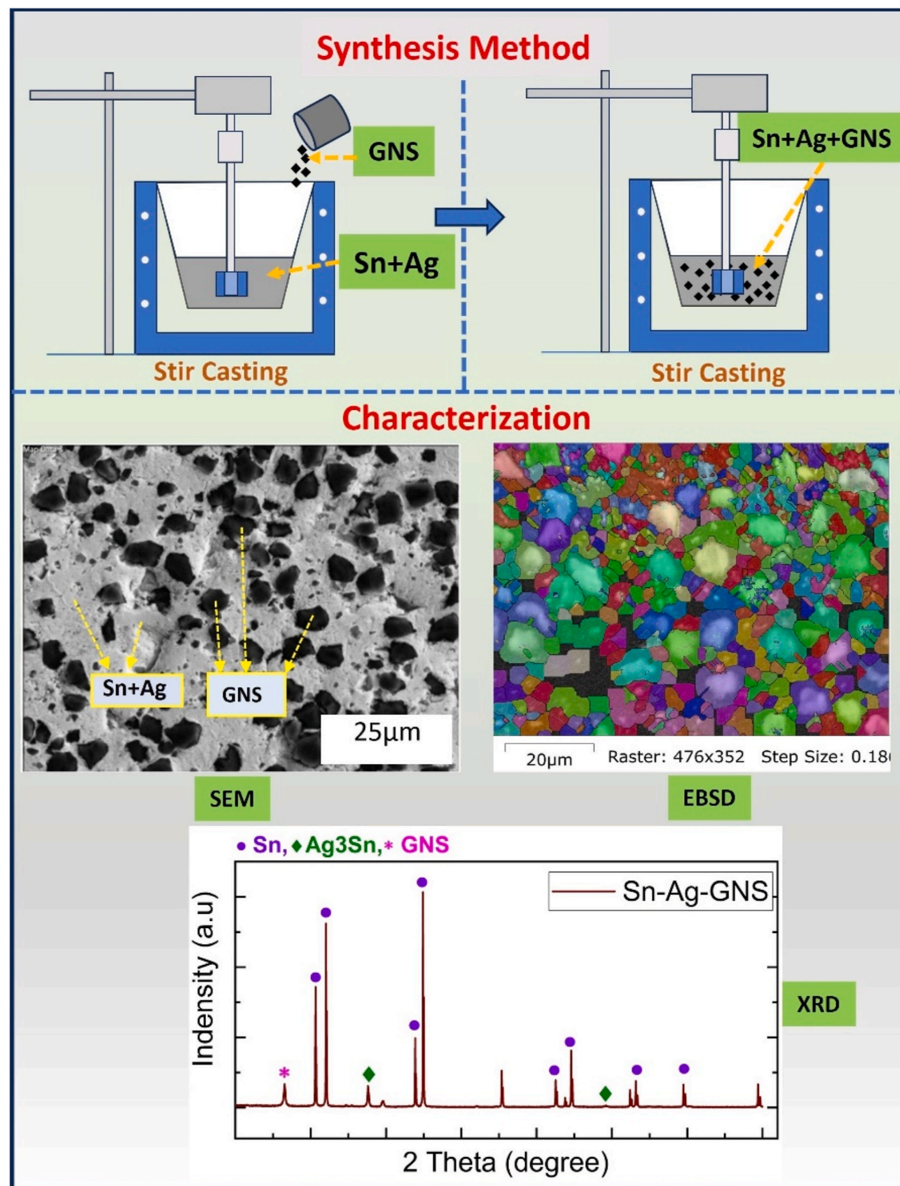

Fig. 1. The whole methodology of the study represented in graphical form.

the solder's mechanical and thermal properties.

2.4. EBSD method

Electron Backscatter Diffraction (EBSD) technique was employed to analyze the crystallographic orientation of the Sn–Ag solder alloys. EBSD analysis was performed on a Symmetry S2® EBSD detector (Oxford Instruments, Abingdon, UK) and Oxford Aztec software. This technique was particularly important for examining the orientation of the Sn phase and the Ag_3Sn intermetallic compounds within the composite. EBSD provided insights into the grain structure, texture, and phase identification, essential for understanding the alloy's mechanical behavior and reliability. The orientation and distribution of the Ag_3Sn phase, as revealed by EBSD, were key factors in assessing the alloy's performance under various thermal and mechanical conditions. The details from the EBSD map enabled a thorough insight on the grain structure by providing clarity on the orientation and distribution of phases, particularly the Ag_3Sn intermetallic, within the Sn–Ag-GNS solder composite. The whole methodology of this study is shown in Fig. 1.

3. Results and discussion

3.1. XRD results

Fig. 2 represents the XRD results obtained for the pure GNS and the Sn–Ag alloy before and after adding GNS. The pattern for the GNS (Fig. 2 (b)) reveal distinct intense peak at lower 2θ value corresponding to reflection from (002) planes of graphene and lower intensity peaks at 48°, 54°, 75° and 86°. The presence of the very intensity peak from (002) planes and few very low intensity peaks indicates the layered structure of the graphene. The pattern for the Sn–Ag alloy depicted in Fig. 2(c) reveals distinct peaks from solid solution of Ag in Sn (Sn) and Ag_3Sn suggesting a multiphase alloy structure containing both phases. The peaks are sharp, indicating good crystallinity of the Sn–Ag alloy. Fig. 2 (a) shows the XRD pattern for the composite revealing peaks corresponding to the reflections from crystallographic planes of Sn phases, Ag_3Sn and GNS. The presence of Sn and Ag peaks in similar positions reveal that GNS has been successfully incorporated into the Sn matrix without significantly altering the crystal structure of the base Sn–Ag alloy. All the peaks of GNS are not distinctly visible is due to the

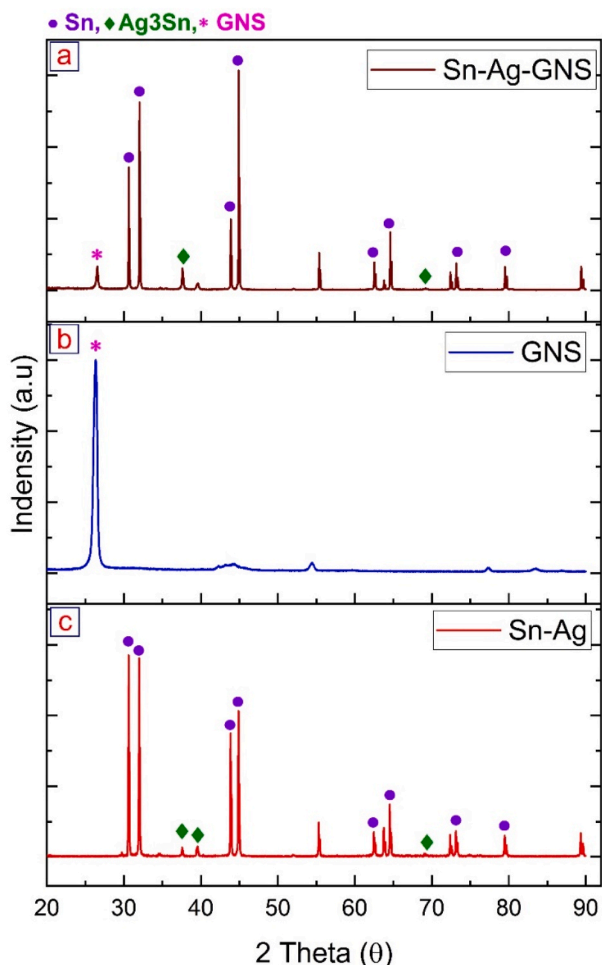

Fig. 2. X-ray diffraction patterns for Sn–Ag solder alloys with and without graphene nanosheets (GNS). (a) XRD pattern of Sn–Ag-GNS composite showing characteristic peaks of tin, silver, and GNS. (b) The XRD pattern for GNS, with a prominent peak indicating the graphene structure. (c) XRD pattern of the Sn–Ag alloy without GNS, showing peaks corresponding to Sn and Ag only.

relatively lower amount of GNS within the Sn matrix. The retention of distinct Sn and Ag_3Sn peaks in the composite suggests that the solder alloy retains its crystalline structure upon the addition of GNS, which is desirable for maintaining the mechanical properties. Fig. 2 (a) reveals variation in the relative intensity of the Sn and Ag_3Sn peaks in the composite material due to the addition of GNS. This indicates the influence the texture or preferred orientation of the crystallites. The absence of new peaks in the composite suggests that GNS does not react to form new phases with Sn or Ag_3Sn during processing of the composite. The GNS could potentially improve the mechanical properties of the Sn–Ag solder by enhancing the strength and conductivity without altering the primary solder microstructure [27,28].

3.2. EBSD before adding GNS

The Electron Backscatter Diffraction (EBSD) results shown in Fig. 3 depict the microstructural characteristics of the Sn–Ag alloy before the addition of Graphene Nano Sheets (GNS). The grain structure, as shown in the first image, demonstrates a diverse grain size distribution with a heterogeneity that is typical of solder alloys without modification or treatment. The image details a significant amount of small grains with a few larger grains interspersed, suggesting a non-uniform microstructure. The grain boundary map complements the grain structure image by highlighting the network of grain boundaries, which is critical for understanding the mechanical properties of the material. Grain boundary characterization can provide insights into the potential pathways for crack propagation and deformation mechanisms. The Pole Figures (PF) and Inverse Pole Figures (IPF) for both tin and silver components (Figs. 4 and 5) indicate the crystallographic orientations of the grains. For instance, the {100}, {110}, and {111} pole figures for silver and tin illustrate a random orientation distribution, which is typical for polycrystalline materials. The intensity of the poles in the pole figures corresponds to texture strength, which has significant implications for the mechanical anisotropy of the material. Furthermore, the histograms of grain size distribution, characterized by pixel count, show that the majority of the grains are small, as evidenced by the high number of counts in the lower pixel count range. The mean grain size, as well as other statistical measures such as the standard deviation, minimum, and maximum, can be directly correlated with the mechanical properties of the material, such as hardness and yield strength [29].

The M-index is low (0.179), which suggest a random texture or weakly textured material. This is an important parameter when considering the workability and anisotropy of the material. The congruence analysis (94% Neighbor Pair - Theoretical, 93% Random Pair - Theoretical, 97% Neighbor Pair - Random Pair) suggests that the actual measured grain boundary character distribution is relatively close to the theoretical distribution for the material.

Analyzing the Orientation Distribution Functions (ODF), ODFs provide a visualization of the preferred crystallographic orientations of the grains in a polycrystalline material. The ODF plots for both Tin (Sn) and Silver (Ag) phases before the addition of GNS show a variation in texture intensity with respect to different φ2 angles, which represent a rotation around the normal to the sample plane. For both Tin and Silver, the intensity of the texture varies with φ2, indicating anisotropy in the material's texture. The texture index is a quantitative measure of the degree of texture, with values for Tin β, Ag_3Sn, and Tin being 5.20, 3.10, and 3.37, respectively. These values suggest that the material exhibits a certain degree of crystallographic texture, which can influence its mechanical anisotropy. The Laue group and sample symmetry information are consistent with the crystal structure of the phases, with Tin β and Ag_3Sn showing tetragonal and orthorhombic symmetries, respectively.

The ODFs (supplementary figure SI Figs. 1–4) also show the intensity of the crystallographic orientations. For instance, Tin β phase presents orientations with a higher intensity at $\varphi 2 = 55^\circ$ and $\varphi 2 = 65^\circ$, while Ag_3Sn phase shows more spread out orientations with moderate intensity peaks. The Laue groups—tetragonal for Tin β and orthorhombic for Ag_3Sn —indicate the symmetry of the crystal structures, which can be correlated to the anisotropy in mechanical properties.

3.3. EBSD after adding GNS

The grain structure image (Fig. 6) shows a dense packing of grains with varying colors representing different orientations. The presence of GNS appears to have refined the grain size, as indicated by a grain count of 558, which is lower compared to the initial state before GNS addition. This refinement might be due to the potential role of GNS as a nucleation site during solidification, promoting the formation of more grains. The mean grain size is 283.4 pixels with an area-weighted mean size of 883.2 pixels. The distribution of grain sizes shows a greater spread with a maximum grain size of 3148 pixels, indicating that while the average grain size is smaller, there are still some larger grains present. This could suggest localized areas of abnormal grain growth. The raster of 476x352 with a step size of 0.1864 μm provides a high-resolution insight into the microstructure, allowing for the detection of finer details compared to pre-GNS addition.

The pole figures for Ag_3Sn (Fig. 7) show a discernible texture with certain orientations appearing more prominently than others. This preferred orientation could be due to directional solidification or mechanical working during processing. The presence of GNS influence the texture of the alloy by altering the grain growth dynamics. This is

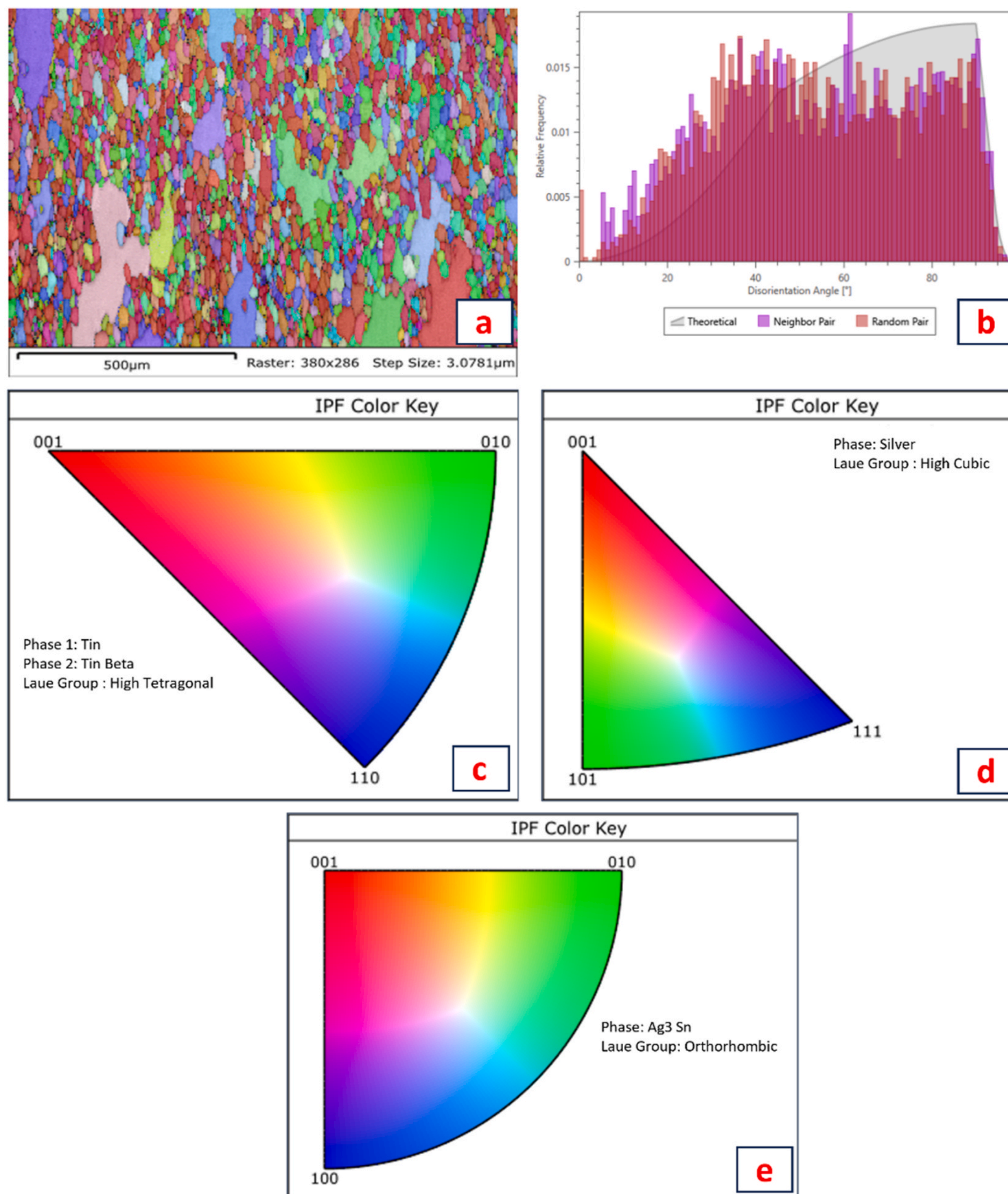

Fig. 3. EBSD characterization of Sn–Ag solder alloy microstructure. (a) EBSD map displaying the crystallographic orientations of the grains in the alloy. (b) Disorientation angle distribution histogram comparing the experimental data with theoretical predictions for both neighbor and random pairs, indicating grain boundary character. (c),(d)and (e) colour keys.

evident in the texture intensity and the distribution of poles, which is an important factor to consider when correlating to the mechanical anisotropy of the material.

Analysing Disorientation Angle Distribution, the distribution shows a significant number of grain boundaries with a lower misorientation angle, which is indicative of an increase in low-angle grain boundaries (LAGBs) [30]. This could contribute to ductility and potentially enhance the fatigue resistance of the material. The M-index has decreased to 0.077 after GNS addition, suggesting a stronger texture as compared to the pre-GNS state. The congruence analysis showing 81% Neighbor Pair - Theoretical and 99% Random Pair - Theoretical confirms that the texture has become more pronounced after GNS addition. There is also a notable decrease in the congruence between Neighbor Pair and Random Pair (80%), suggesting that the GNS addition has influenced the grain boundary character distribution away from a random polycrystalline structure [30].

The grain size histogram post-GNS addition shows a bimodal distribution with peaks at both the smaller and larger grain sizes. The presence of a bimodal distribution usually indicates that different mechanisms might be controlling the grain growth, with the possibility of pinning effects due to the GNS. The standard deviation of grain sizes has increased to 412.6 pixels, further confirming the wider spread in grain sizes and suggesting a more heterogeneous grain structure. The reduction in the mean grain size with GNS addition could be linked to potential improvements in yield strength through the Hall-Petch relationship [31]. The change in texture, as evidenced by the pole figures and the M-index, could be correlated with alterations in mechanical anisotropy, which would be critical for the reliability of solder joints in thermal and mechanical service conditions [32].

The bimodal distribution of grain sizes observed in the Sn–Ag alloy post the addition of GNS suggests the presence of two distinct populations of grains: smaller grains, which could be associated with the

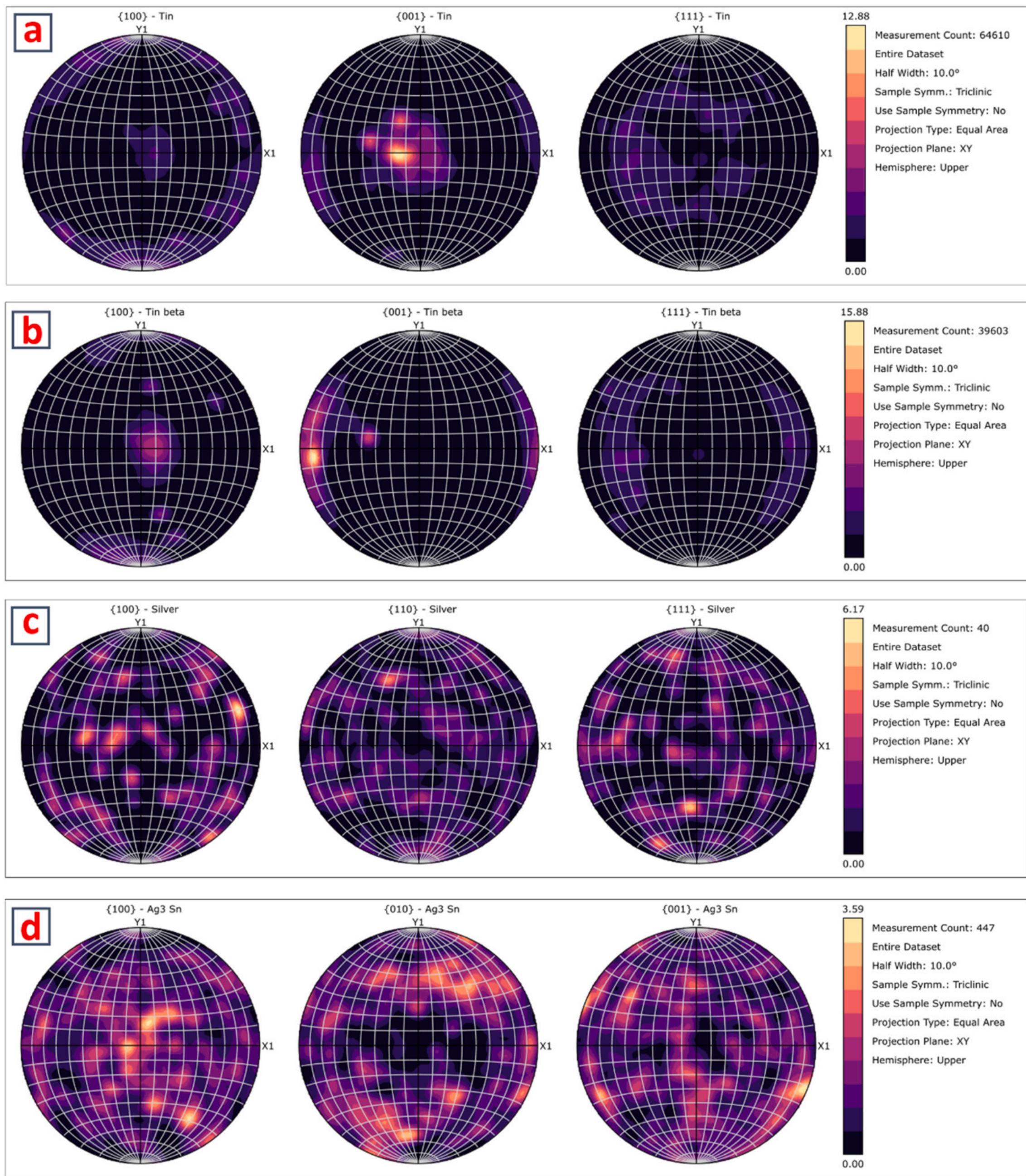

Fig. 4. Pole figure representations of crystallographic texture for different phases in the Sn–Ag solder alloy. (a) Pole figures for pure tin (α-Sn) showing the orientation distribution of the {100}, {001}, and {111} planes. (b) Pole figures for the tin beta (β-Sn) phase indicating the texture of the {100}, {001}, and {111} planes. (c) Pole figures for pure silver (Ag) displaying the orientation distribution for the {100}, {110}, and {111} planes. (d) Pole figures for the Ag_3Sn intermetallic compound illustrating the texture of the {100}, {010}, and {001} planes.

Zener pinning effect caused by the GNS, and larger grains that managed to grow before encountering the pinning particles or in regions with a lower density of GNS. The introduction of GNS have provided additional nucleation sites, leading to a higher number of grains initiating from these sites. This increase in nucleation sites can result in a larger population of smaller grains, as more grains begin to grow simultaneously, limiting the overall space and resources available for each to expand. Relating it to the Zener Pinning Effect, GNS particles can act as pinning agents at the grain boundaries, resisting their movement during recrystallization and grain growth. This pinning effect can stabilize the smaller grains by hindering the growth of existing grains. The Zener pinning effect is a phenomenon where particles within the matrix exert a drag force on the grain boundaries, which increases with decreasing particle spacing.

The IPFs (Fig. 8) for Ag_3Sn and Graphite phases show specific orientation clusters, which are indicative of texture components that have developed during processing. The IPFs are a direct visualization of the preferred crystallographic orientations of grains relative to the sample reference frame. In the Ag_3Sn phase, the intensity of the pole figures (max of 7.86) suggests a relatively strong texture, which can be attributed to the influence of GNS on the solidification process, possibly by providing nucleation sites that encourage certain orientations. The IPF for Graphite shows a significant intensity (max of 16.36), indicating a strong preferential alignment of graphite flakes. This could potentially influence the mechanical properties by reinforcing the material along certain planes and directions. The Silver phase demonstrates lower

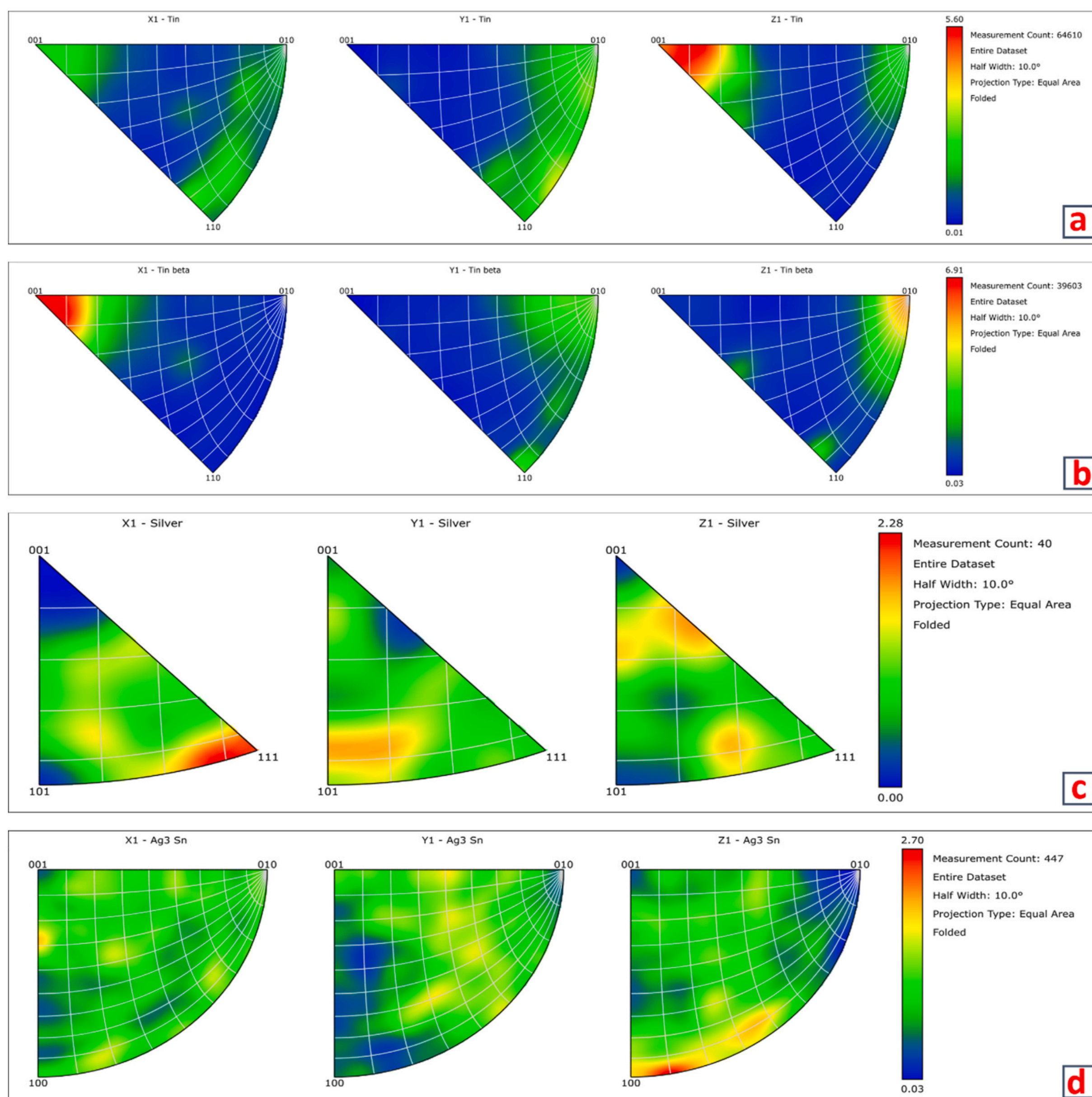

Fig. 5. Inverse pole figure (IPF) maps showing crystallographic orientation distributions for individual phases within a Sn–Ag solder alloy. (a) IPF maps for pure tin (α-Sn) across three orthogonal directions: X1, Y1, and Z1. (b) IPF maps for the tin beta (β-Sn) phase, similarly across the X1, Y1, and Z1 directions. (c) IPF maps for pure silver (Ag), demonstrating the crystal orientation distribution in the X1, Y1, and Z1 directions. (d) IPF maps for the intermetallic phase Ag_3Sn, presented for the same three orthogonal directions.

texture intensities (max of 5.06) compared to the other two phases, suggesting a more random crystallographic orientation distribution within this phase [33,34].

The ODFs (supplementary figure SI Figs. 5–9) provide a quantitative measure of texture by illustrating the distribution of crystallographic orientations in a 3D space of Euler angles. For the Tin phase, the ODF reveals a noticeable texture with a max intensity of 17.34, highlighting the presence of certain orientations that are more prevalent. The texture index of 3.78 points to a moderate texture strength. The Ag_3Sn phase ODF shows a very strong texture with a max intensity of 85.52 and a texture index of 12.13, indicating a significant influence of GNS on the crystallographic orientation distribution. The strong texture can be linked to directional solidification influences or other processing conditions [27]. The ODF for Graphite shows an exceptionally high texture intensity (max of 239.26) with a texture index of 20.07, suggesting a very pronounced alignment of the graphite phase [28].

The integration of GNS within the Sn–Ag alloy has had a marked impact on the microstructural and textural characteristics of the material. GNS acts as a heterogeneous nucleation site, influencing grain orientation during solidification and potentially altering mechanical properties through texture strengthening. The strong textures observed in the IPFs and ODFs for the Ag_3Sn and Graphite phases suggest that the addition of GNS lead to anisotropic mechanical behavior, which can be beneficial for certain applications where directional properties are desired. For instance, the alignment of GNS could enhance the thermal conductivity along specific planes, which is beneficial for thermal management applications in electronics [20]. The lower texture intensity in the Silver phase contribute to maintaining a balance between strength and ductility, as highly textured materials can sometimes exhibit brittleness along certain planes [35].

Without GNS, The disorientation angle distribution lean towards higher angles, suggesting that there is a significant grain growth post-

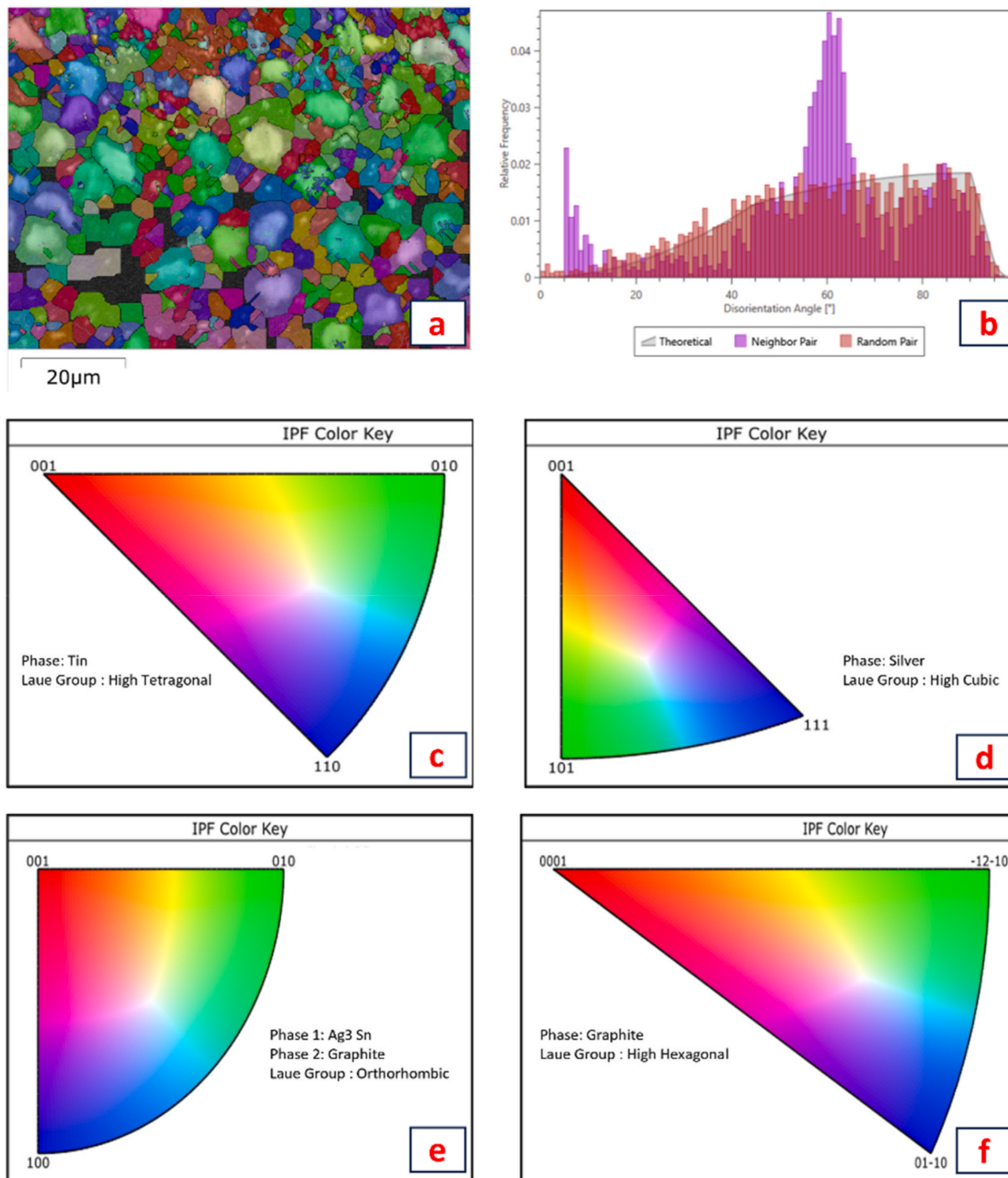

Fig. 6. EBSD analysis of a multi-phase Sn–Ag solder alloy containing GNS. (a) EBSD map showcasing the microstructural grain orientation within the alloy. (b) Grain boundary misorientation angle distribution histogram, with color coding that distinguishes between theoretical, neighbor pair, and random pair disorientation angles. (c),(d)and (e) colour keys.

nucleation that contributes to the formation of high-angle grain boundaries. With GNS, The distribution of disorientation angles show a shift towards lower angles, implying that GNS restricts grain growth and maintains a higher population of low-angle grain boundaries. The quantitative measure of this is the misorientation index, which generally decreases in the presence of GNS.

Without GNS, the phases present in the Sn–Ag alloy have a more homogeneous distribution, with Ag_3Sn intermetallic compounds typically forming at grain boundaries or as dispersed precipitates within the grains. GNS affect the phase distribution by acting as heterogeneous sites for the precipitation of intermetallic compounds. This could lead to a more heterogeneous distribution of Ag_3Sn phases, which can be quantified by the area fraction and number density of these phases in the EBSD phase maps.

A smaller fraction of low-energy, coincident site lattice (CSL) boundaries is observed, as the grain growth is less restricted. The addition of GNS can lead to an increase in the fraction of CSL boundaries due to restricted grain boundary migration. This can be quantitatively assessed by the fraction of Σ3, Σ9, Σ27, and other CSL boundaries in the grain boundary character distribution (GBCD).

EBSD analysis of Sn–Ag solder alloys before and after the addition of Graphene Nano Sheets (GNS) reveals a significant microstructural evolution. Prior to GNS addition, the EBSD maps depict a heterogeneous grain distribution with a balanced mix of low and high angle grain boundaries, indicative of a material with no strong preferential crystallographic orientation. Upon GNS incorporation, the EBSD images show a refined grain structure, suggesting increased nucleation. There appears to be a shift towards a greater prevalence of low angle grain boundaries, which is likely due to the pinning effect of GNS inhibiting grain growth. This microstructural refinement is expected to enhance mechanical properties, such as yield strength and ductility, while also potentially improving resistance to thermal fatigue—a critical factor for solder joint reliability in electronic components [28,36].

The Kernel Average Misorientation (KAM) map (shown in Fig. 9) for

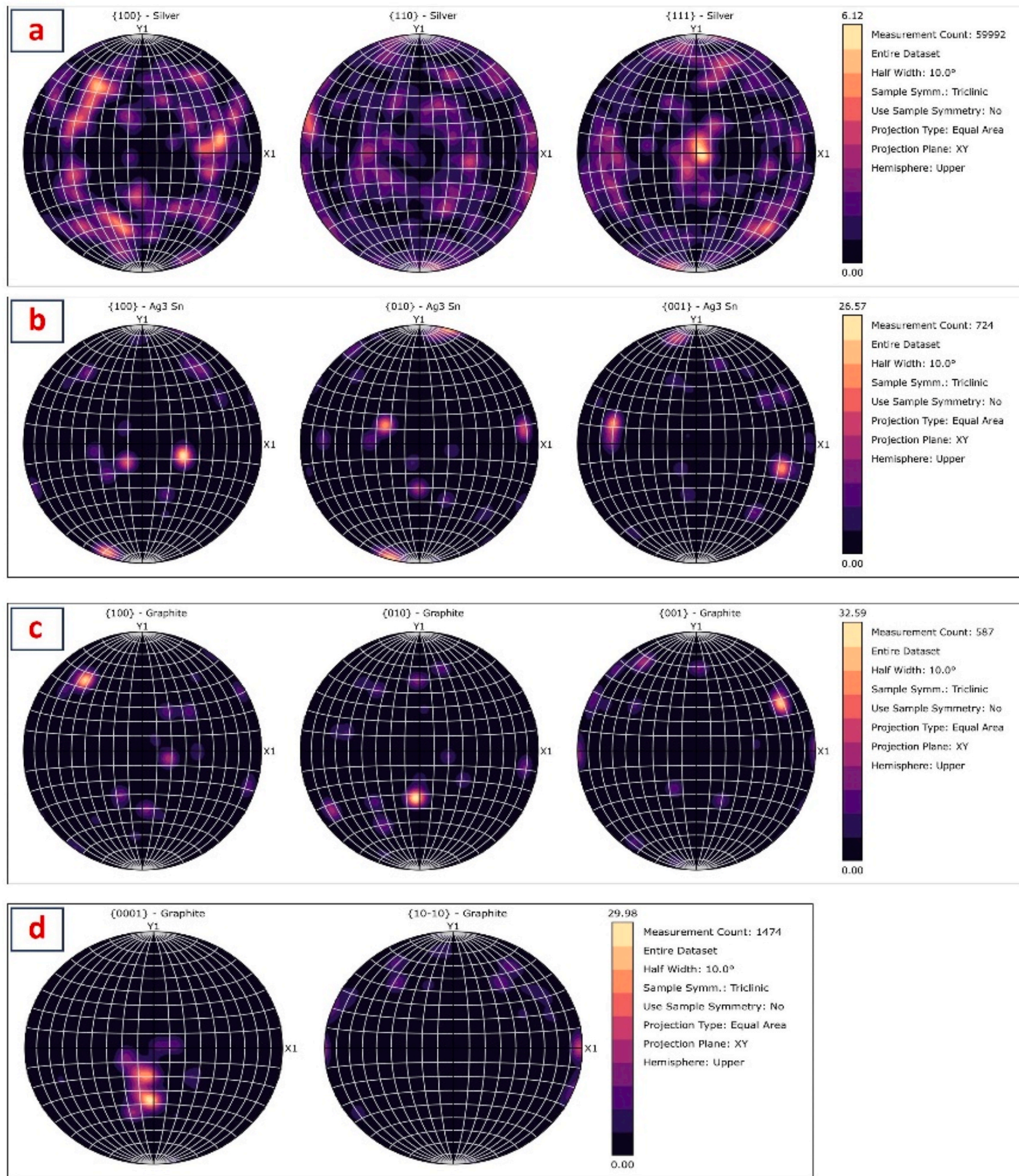

Fig. 7. Pole figure analyses of different phases in a Sn–Ag-graphite solder alloy. (a) Pole figures for the silver (Ag) phase, showing the orientation distribution of {100}, {110}, and {111} planes. (b) Pole figures for the Ag_3Sn intermetallic phase, illustrating the texture of {100}, {010}, and {001} planes. (c) Pole figures for graphite phase in the hexagonal crystal system, presenting the orientation distribution for {100}, {010}, and {001} planes. (d) Additional pole figures for the graphite phase, with emphasis on the basal {0001} plane and the prismatic {10-10} plane.

the Sn–Ag-GNS solder alloy shows local misorientation ranging from 0 to nearly 5°. Low-strain regions, represented by the prevalent blue areas, indicate less deformed grains with KAM values close to 0. The sporadic green to yellow regions highlight moderate strains, with KAM values ascending towards the middle of the range, likely due to the presence of GNS acting as dislocation barriers. The occasional red spots, where KAM values approach 5°, pinpoint significant local strains, corresponding to areas of intense stress concentration around GNS or at grain boundaries. This distribution underscores the heterogeneity of the strain field within the material, influenced by the incorporation of GNS [37].

3.4. SEM, EDS and colour mapping

Before GNS Addition (Fig. 10), The SEM image shows a relatively homogeneous microstructure with smooth features and uniform distribution, typical of Sn–Ag alloys without additional reinforcement. The SEM images show that, after the addition of GNS (Fig. 11), the grain morphology changes from uniform pre-addition grains with average sizes around 10 μm to a bimodal distribution with average sizes varying from 2 μm to 20 μm The color mappings are consistent and evenly distributed, reflecting the homogeneity of the alloy elements. Color mapping via EDS highlights the distribution of GNS, showing a stark contrast in the elemental distribution. The weight percentage of GNS is 47 in the composite. For example, tin's even distribution becomes

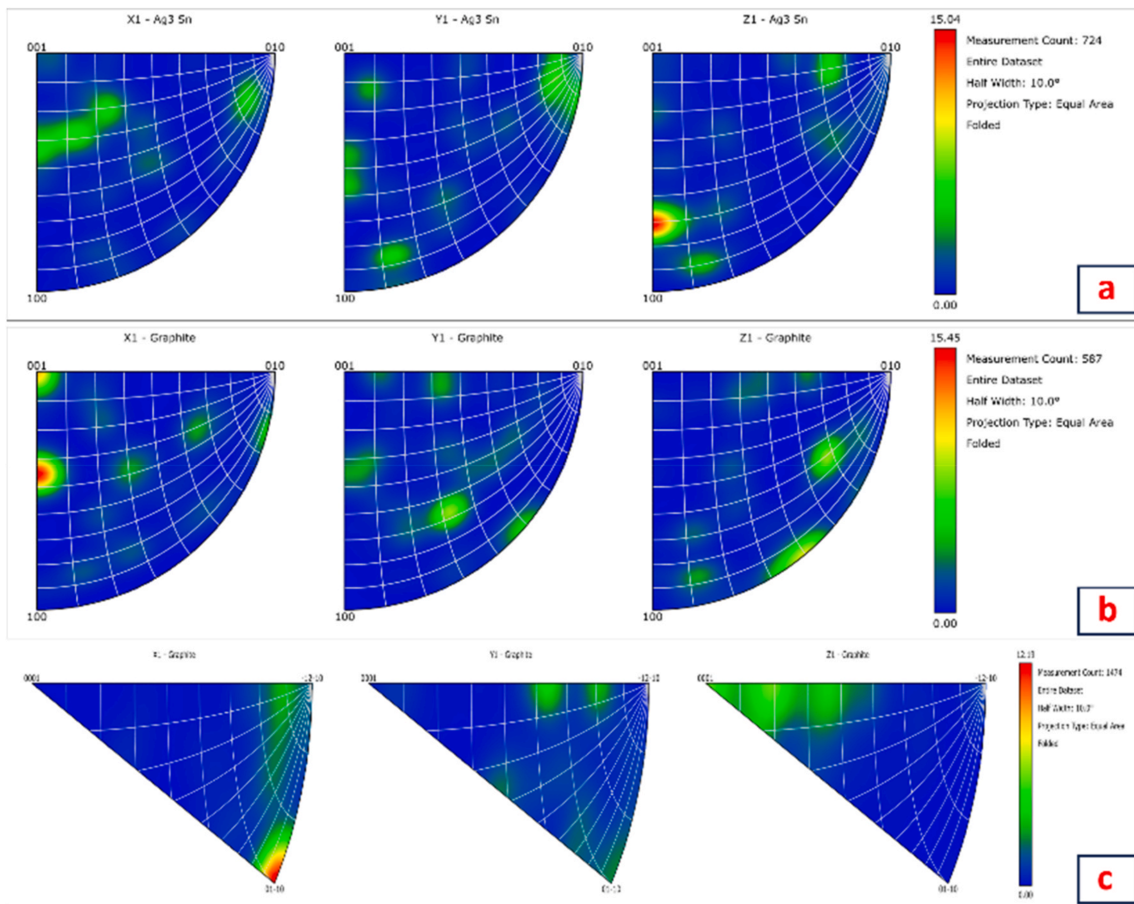

Fig. 8. Inverse pole figure (IPF) maps for the Ag_3Sn intermetallic and graphite phases in a Sn–Ag solder alloy. (a) IPF maps for the Ag_3Sn phase across three orthogonal planes: X1, Y1, and Z1, showing the orientation distribution of the crystal lattice. (b) IPF maps for graphite, highlighting orientation distribution in the X1, Y1, and Z1 directions. (c) IPF maps for graphite focusing on the basal and prismatic planes.

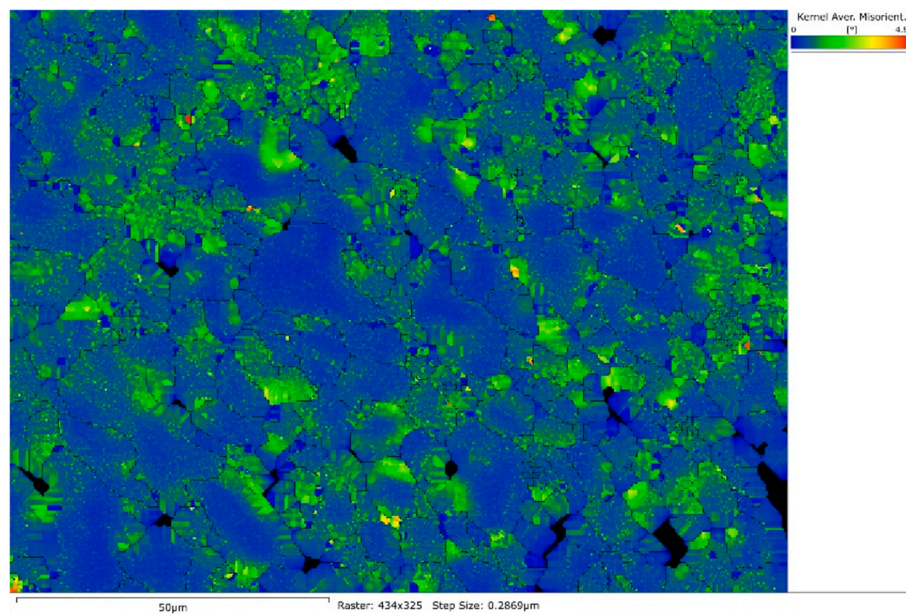

Fig. 9. Kernel Average Misorientation (KAM) map of a Sn–Ag solder alloy reinforced with Graphene Nano Sheets (GNS). The color scale indicates the degree of local misorientation within the alloy, ranging from 0 (blue) to approximately 5° (red).

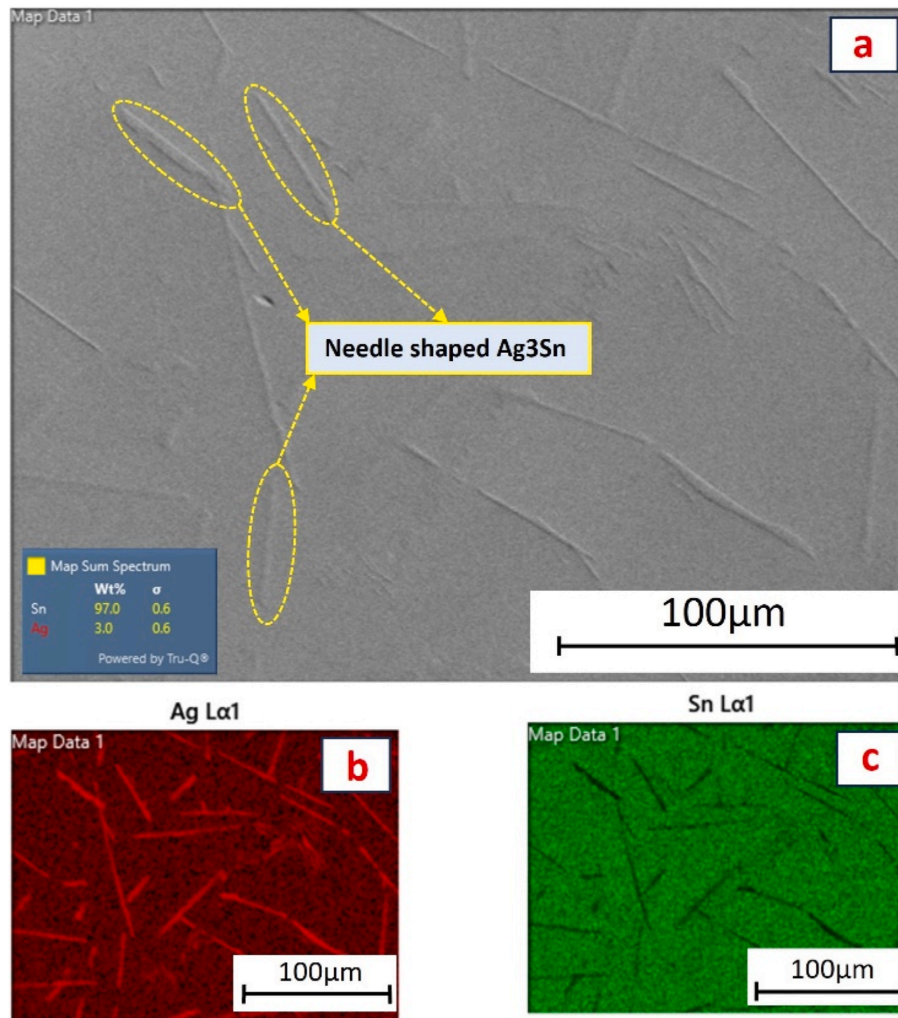

Fig. 10. SEM and EDS analysis of Sn–Ag solder alloy. (a) SEM image highlighting needle-shaped Ag_3Sn intermetallic compounds within the Sn matrix, delineated by yellow dashed lines. The inset shows the EDS spectrum with quantitative elemental analysis, indicating the weight percentage of Sn and Ag in the analyzed area. (b) EDS mapping for silver (Ag), where the red intensity indicates the distribution and concentration of Ag elements. (c) EDS mapping for tin (Sn), with the green intensity representing the distribution and concentration of Sn elements.

interspersed with carbon-rich areas, where the carbon mapping post-GNS addition shows a dense population of green pixels indicative of GNS clusters. After GNS Addition, the microstructure becomes more heterogeneous with distinct black regions indicative of GNS agglomerations within the Sn–Ag matrix. These regions interrupt the continuity of the matrix, which can affect the mechanical properties by providing sites for stress concentration. The green and red color mappings representing different elements (Sn and Ag) are disrupted by the presence of GNS, as evidenced by the areas of contrasting colors. These mappings show the distribution of GNS within the alloy and suggest that GNS clusters act as barriers to the movement of dislocations, potentially enhancing the strength of the material. The addition of GNS creates a composite microstructure where GNS particles are distributed throughout the Sn–Ag matrix. This distribution is critical as it influences the overall mechanical properties of the alloy. The Sn and Ag elements in the solder alloy without GNS are evenly distributed, as expected in a well-mixed alloy. The addition of GNS disrupts this homogeneity, which can lead to localized variations in mechanical properties.

The inclusion of GNS within the Sn–Ag solder alloy could be advantageous for applications that require enhanced mechanical properties and efficient heat dissipation.

4. Conclusion

The EBSD, SEM, and EDS results collectively indicate that GNS addition has a profound impact on the microstructural and compositional characteristics of the Sn–Ag alloy. While the addition of GNS enhances the carbon content quantitatively, it disrupts the previously uniform distribution of Sn and Ag, as seen in the SEM images and color mappings. EBSD results suggest that the introduction of GNS affects the grain structure, possibly leading to texture changes that could influence mechanical properties such as strength and ductility. EBSD results could show a reduction in average grain size and a shift towards a more complex texture. This could be directly correlated with Sn–Ag-GNS composite suitable for high-performance electronic applications. However, the potential for GNS agglomeration poses a challenge for maintaining uniform mechanical properties across the alloy. The quantitative assessment of grain sizes before and after GNS addition reveals a bimodal distribution in the latter, with the presence of both finer and coarser grains. The average grain size has decreased, with smaller grains potentially leading to higher mechanical strength due to grain boundary strengthening mechanisms. The texture index, a quantitative measure of crystallographic texture, shows a variation indicative of the changes in anisotropy within the material. A higher texture index after GNS addition suggests a more pronounced crystallographic orientation, which

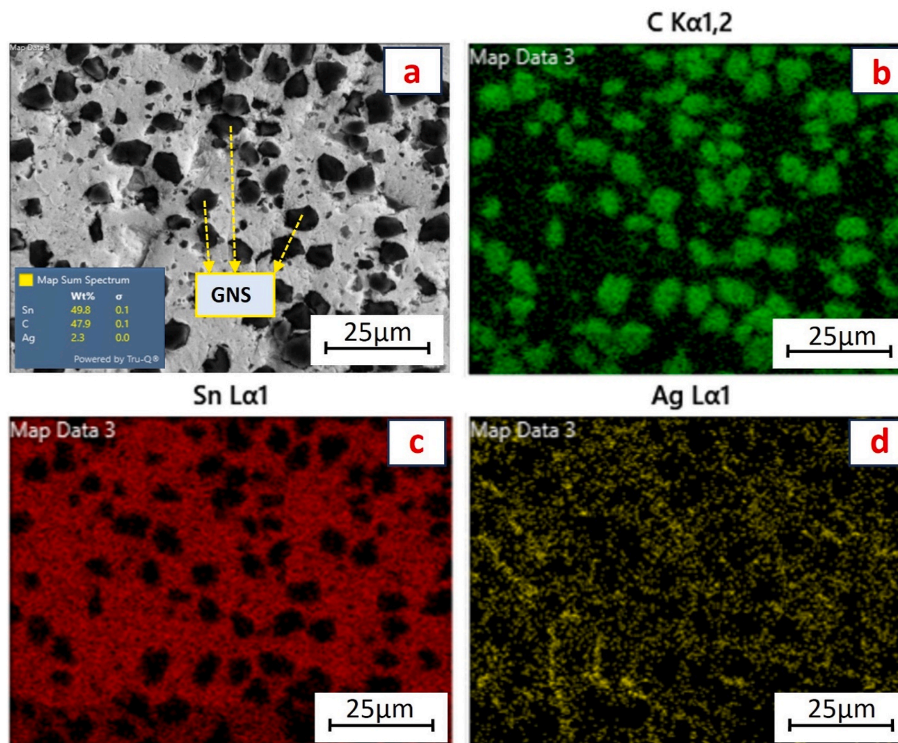

Fig. 11. SEM image and corresponding EDS elemental maps of a Sn–Ag-GNS composite. (a) SEM image showing the distribution of GNS within the composite matrix, with EDS quantitative analysis inset displaying weight percentages for Sn, C, and Ag. (b) EDS map for carbon (C) indicating the presence and distribution of GNS. (c) EDS map for tin (Sn) showing the distribution of Sn within the composite. (d) EDS map for silver (Ag) highlighting the distribution of Ag particles.

can influence the anisotropy in mechanical and thermal properties. EBSD results show a stark transformation in the grain boundary character. The fraction of high-angle grain boundaries increases from approximately 55% pre-GNS addition to 75% post-GNS addition. The texture index escalates from about 3.5 to 8.0, indicating a substantial increase in preferred orientation alignment. The effect of GNS on grain boundary scattering could influence both the electrical and thermal conductivity of the alloy. The impact would depend on the distribution and orientation of the GNS within the matrix. As a future recommendation more analysis has to be completed on the electrical and thermal behavior of this composite.

Data availability

The raw/processed data required to reproduce these findings cannot be shared at this time as the data also forms part of an ongoing study.

Declaration of generative AI and AI-assisted technologies in the writing process

During the preparation of this work the authors used ChatGPT to rephrase the literature and improving language. After using this tool/service, the authors reviewed and edited the content as needed and take full responsibility for the content of the publication.

Declaration of competing interest

The authors declare that they have no known competing financial interests or personal relationships that could have appeared to influence the work reported in this paper.

Acknowledgements

This research did not receive any specific grant from funding agencies in the public, commercial, or not-for-profit sectors. The authors would like to thank Mr. Colin Thorneycroft, Development Officer - Manufacturing, Materials, and Metrology at Coventry University, for his help and support in conducting the experiments.

Appendix A. Supplementary data

Supplementary data to this article can be found online at https://doi.org/10.1016/j.jmrt.2024.04.043.

References

[1] Suganuma K. "Advances in lead-free electronics soldering,". Curr Opin Solid State Mater Sci Jan. 2001;5(1):55–64. https://doi.org/10.1016/S1359-0286(00)00036-X.

[2] Adetunji OR, Ashimolowo RA, Aiyedun PO, Adesusi OM, Adeyemi HO, Oloyede OR. "Tensile, hardness and microstructural properties of Sn-Pb solder alloys,". Mater Today Proc Jan. 2021;44:321–5. https://doi.org/10.1016/J.MATPR.202009.656.

[3] Abtew M, Selvaduray G. "Lead-free Solders in Microelectronics,". Mater Sci Eng R Rep Jun. 2000;27(5–6):95–141. https://doi.org/10.1016/S0927-796X(00)00010-3.

[4] Jayesh S, Elias J. "Experimental Investigation on the Effect of Ag Addition on Ternary Lead Free Solder Alloy –Sn–0.5Cu–3Bi,". Met Mater Int 2020;26(1):107–14. https://doi.org/10.1007/s12540-019-00305-3.

[5] Hedemann-Robinson M. "The EU Directives on Waste Electrical and Electronic Equipment and on the Restriction of Use of Certain Hazardous Substances in Electrical and Electronic Equipment: Adoption Achieved,". Eur Environ Law Rev 2003:52–60 [Online]. Availablehttp://www.kluwerlawonline.com/api/Product/CitationPDFURL?file=Journals\EELR\EELR2003007.pdf.

[6] Liu Y, Tu KN. "Low melting point solders based on Sn, Bi, and In elements,". Mater Today Adv Dec. 2020;8:100115. https://doi.org/10.1016/J.MTADV.2020100115.

[7] Wang F, Chen H, Huang Y, Liu L, Zhang Z. "Recent progress on the development of Sn–Bi based low-temperature Pb-free solders," *Journal of Materials Science*. Materials in Electronics 2019;30(4):3222–43. https://doi.org/10.1007/s10854-019-00701-w.

[8] Zhang L, Liu Z. "Inhibition of intermetallic compounds growth at Sn–58Bi/Cu interface bearing CuZnAl memory particles (2–6 μm)," *Journal of Materials Science*. Materials in Electronics 2020;31(3):2466–80. https://doi.org/10.1007/s10854-019-02784-x.

[9] Liu S, Xue S, Xue P, Luo D. "Present status of Sn–Zn lead-free solders bearing alloying elements," *Journal of Materials Science*. Materials in Electronics 2015;26 (7):4389–411. https://doi.org/10.1007/s10854-014-2659-7.

[10] Hadian F, Schoeller H, Cotts E. "Correlation Between the Growth of Voids and Ni3Sn4 Intermetallic Compounds at SnAg/Ni and SnAgCuBiSbNi/Ni Interfaces at Temperatures up to 200°C,". J Electron Mater 2020;49(1):226–40. https://doi.org/10.1007/s11664-019-07727-0.

[11] Jayesh S, Elias J. "Experimental Investigation on the Effect of Ag Addition on Ternary Lead Free Solder Alloy –Sn–0.5Cu–3Bi,". Met Mater Int 2020;26(1): 107–14. https://doi.org/10.1007/s12540-019-00305-3.

[12] Xiong M, Zhang L. "Interface reaction and intermetallic compound growth behavior of Sn-Ag-Cu lead-free solder joints on different substrates in electronic packaging,". J Mater Sci 2019;54(2):1741–68. https://doi.org/10.1007/s10853-018-2907-y.

[13] Sharma A, Sohn H-R, Jung JP. "Effect of Graphene Nanoplatelets on Wetting, Microstructure, and Tensile Characteristics of Sn-3.0Ag-0.5Cu (SAC) Alloy,". Metall Mater Trans 2016;47(1):494–503. https://doi.org/10.1007/s11661-015-3214-8.

[14] Illés B, et al. "Dispersion and incorporation of TiO2 and SiC nano-particles in SAC alloy. SIMS and DFT study," Scr Mater Apr. 2024;243:115987. https://doi.org/10.1016/J.SCRIPTAMAT.2024115987.

[15] Mohd Nasir SS, Yahaya MZ, Erer AM, Illés B, Mohamad AA. "Effect of TiO2 nanoparticles on the horizontal hardness properties of Sn-3.0Ag-0.5Cu-1.0TiO2 composite solder,". Ceram Int Oct. 2019;45(15):18563–71. https://doi.org/10.1016/J.CERAMINT.201906.079.

[16] Choi H, Illés B, Hurtony T, Byun J, Géczy A, Skwarek A. "Corrosion problems of SAC-SiC composite solder alloys,". Corrosion Sci Nov. 2023;224:111488. https://doi.org/10.1016/J.CORSCI.2023111488.

[17] Skwarek A, Illés B, Górecki P, Pietruszka A, Tarasiuk J, Hurtony T. "Influence of SiC reinforcement on microstructural and thermal properties of SAC0307 solder joints,". J Mater Res Technol Jan. 2023;22:403–12. https://doi.org/10.1016/J.JMRT.202211.126.

[18] Skwarek A, et al. "Application of ZnO Nanoparticles in Sn99Ag0.3Cu0.7-Based Composite Solder Alloys," *Nanomaterials*, 2021;11(no. 6). https://doi.org/10.3390/nano11061545.

[19] Yahaya MZ, Nazeri MFM, Kheawhom S, Illés B, Skwarek A, Mohamad AA. Microstructural analysis of Sn-3.0Ag-0.5Cu-TiO2 composite solder alloy after selective electrochemical etching. Mater Res Express Jan. 2020;7(1):16583. https://doi.org/10.1088/2053-1591/ab6b57.

[20] Li Y, et al. A Review on the Development of Adding Graphene to Sn-Based Lead-Free Solder. Metals 2023;13(no. 7). https://doi.org/10.3390/met13071209.

[21] Qian Y, Hwang S, Lee J, Seo JS, Baeck SH, Shim SE. "Novel electroless plating of silver nanoparticles on graphene nanoplatelets and its application for highly conductive epoxy composites,". J Ind Eng Chem Apr. 2021;96:156–62. https://doi.org/10.1016/J.JIEC.202101.014.

[22] Kim Y, et al. "Strengthening effect of single-atomic-layer graphene in metal–graphene nanolayered composites,". Nat Commun 2013;4(1):2114. https://doi.org/10.1038/ncomms3114.

[23] Wang J, Li Z, Fan G, Pan H, Chen Z, Zhang D. "Reinforcement with graphene nanosheets in aluminum matrix composites,". Scripta Mater Apr. 2012;66(8): 594–7. https://doi.org/10.1016/J.SCRIPTAMAT.201201.012.

[24] Ma Y, et al. "Effects of graphene nanosheets addition on microstructure and mechanical properties of SnBi solder alloys during solid-state aging,". Mater Sci Eng Jun. 2017;696:437–44. https://doi.org/10.1016/J.MSEA.201704.105.

[25] Huang Y, Xiu Z, Wu G, Tian Y, He P. "Sn–3.0Ag–0.5Cu nanocomposite solders reinforced by graphene nanosheets," *Journal of Materials Science*. Materials in Electronics 2016;27(7):6809–15. https://doi.org/10.1007/s10854-016-4631-1.

[26] Eray S. "Application of metal oxides in composites,". Metal Oxide Powder Technologies: Fundamentals, Processing Methods and Applications Jan. 2020: 101–19. https://doi.org/10.1016/B978-0-12-817505-7.00006-3.

[27] Sharma A, Sohn H-R, Jung JP. Effect of Graphene Nanoplatelets on Wetting, Microstructure, and Tensile Characteristics of Sn-3.0Ag-0.5Cu (SAC) Alloy. Metall Mater Trans 2016;47(1):494–503. https://doi.org/10.1007/s11661-015-3214-8.

[28] Kim Y, et al. "Strengthening effect of single-atomic-layer graphene in metal–graphene nanolayered composites,". Nat Commun 2013;4(1):2114. https://doi.org/10.1038/ncomms3114.

[29] Li Y, Bushby AJ, Dunstan DJ. "The Hall–Petch effect as a manifestation of the general size effect," *Proceedings of the Royal Society A*. Math Phys Eng Sci 2016;472 (2190):20150890. https://doi.org/10.1098/rspa.2015.0890.

[30] Telang AU, et al. Grain-boundary character and grain growth in bulk tin and bulk lead-free solder alloys. J Electron Mater 2004;33(12):1412–23. https://doi.org/10.1007/s11664-004-0081-2.

[31] Cordero ZC, Knight BE, Schuh CA. "Six decades of the Hall–Petch effect – a survey of grain-size strengthening studies on pure metals,". Int Mater Rev Nov. 2016;61 (8):495–512. https://doi.org/10.1080/09506608.2016.1191808.

[32] Z.-Q. L. L. S. W.-M. L. P. H. M.-Y. X. Nan Jiang Liang Zhang and M. Zhao. "Reliability issues of lead-free solder joints in electronic devices,". Sci Technol Adv Mater 2019;20(1):876–901. https://doi.org/10.1080/14686996.2019.1640072.

[33] Stankovich S, et al. "Graphene-based composite materials,". Nature 2006;442 (7100):282–6. https://doi.org/10.1038/nature04969.

[34] Young RJ, Kinloch IA, Gong L, Novoselov KS. "The mechanics of graphene nanocomposites: A review,". Compos Sci Technol Jul. 2012;72(12):1459–76. https://doi.org/10.1016/J.COMPSCITECH.201205.005.

[35] Horita Z, Ohashi K, Fujita T, Kaneko K, Langdon TG. "Achieving High Strength and High Ductility in Precipitation-Hardened Alloys,". Adv Mater 2005;17(13): 1599–602. https://doi.org/10.1002/adma.200500069.

[36] Li Y, et al. A Review on the Development of Adding Graphene to Sn-Based Lead-Free Solder. Metals 2023;13(no. 7). https://doi.org/10.3390/met13071209.

[37] Chen H, Yan B, Yang M, Ma X, Li M. "Effect of grain orientation on mechanical properties and thermomechanical response of Sn-based solder interconnects,". Mater Charact, Nov. 2013;85:64–72. https://doi.org/10.1016/J.MATCHAR.201307.004.